ACS Energy LETTERS

http://pubs.acs.org/journal/aelccp

LETTER

15.3%-Efficient GaAsP Solar Cells on GaP/Si Templates

Michelle Vaisman,[†,‡] Shizhao Fan,[§] Kevin Nay Yaung,[†] Emmett Perl,[‡] Diego Martín-Martín,[∥] Zhengshan J. Yu,[⊥] Mehdi Leilaeioun,[⊥] Zachary C. Holman,[⊥] and Minjoo L. Lee*[,§]

[†]Department of Electrical Engineering, Yale University, New Haven, Connecticut 06511, United States

[‡]National Renewable Energy Laboratory, Golden, Colorado 80401, United States

[§]Department of Electrical and Computer Engineering, University of Illinois Urbana−Champaign, Urbana, Illinois 61801, United States

[∥]Área de Tecnología Electrónica, Universidad Rey Juan Carlos, Móstoles, Madrid 28933, Spain

[⊥]School of Electrical, Computer and Energy Engineering, Arizona State University, Tempe, Arizona 85287, United States

Supporting Information

ABSTRACT: As single-junction Si solar cells approach their practical efficiency limits, a new pathway is necessary to increase efficiency in order to realize more cost-effective photovoltaics. Integrating III−V cells onto Si in a multijunction architecture is a promising approach that can achieve high efficiency while leveraging the infrastructure already in place for Si and III−V technology. In this Letter, we demonstrate a record 15.3%-efficient 1.7 eV GaAsP top cell on GaP/Si, enabled by recent advances in material quality in conjunction with an improved device design and a high-performance antireflection coating. We further present a separate Si bottom cell with a 1.7 eV GaAsP optical filter to absorb most of the visible light with an efficiency of 6.3%, showing the feasibility of monolithic III−V/Si tandems with >20% efficiency. Through spectral efficiency analysis, we compare our results to previously published GaAsP and Si devices, projecting tandem GaAsP/Si efficiencies of up to 25.6% based on current state-of-the-art individual subcells. With the aid of modeling, we further illustrate a realistic path toward 30% GaAsP/Si tandems for high-efficiency, monolithically integrated photovoltaics.

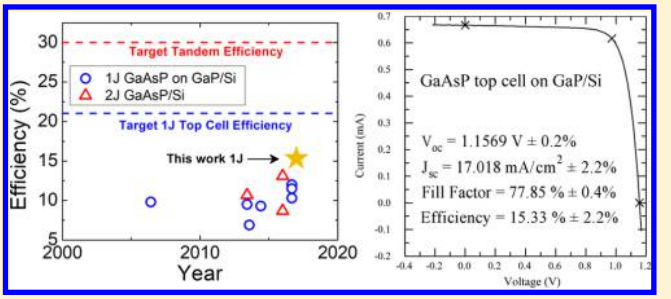

Silicon has been the primary commercial photovoltaic (PV) technology for multiple decades. Consequently, it is comparatively well understood and has a well-developed infrastructure. However, in order to enhance the widespread adoption of PV as a major energy source, the cost of PV needs to be reduced; current average utility-scale PV costs of ∼$0.04−0.10/kWh require significant improvement to reach the SunShot 2030 target of $0.03/kWh.[1] While improving the efficiency (η) of Si PV has been one of the primary methods of reducing balance-of-systems costs commercially, this effort may soon come to a head; current monocrystalline silicon cell efficiencies (26.7%)[2] are quickly approaching the theoretical (29.4%)[3] efficiency limit for single-junction (1J) Si cells. Si-based tandems can enable efficiencies beyond 1J Si cells while simultaneously benefiting from the low cost of Si and its extensive infrastructure. In particular, perovskites have been of great interest as a potential top cell material, demonstrating marked advancements in achieving high-efficiency solar cells with bandgaps appropriate for tandem architectures.[4−12] However, Si, CdTe, CIGS, and III−Vs are the only technologies that have demonstrated the 25+ year lifespans necessary for commercial deployment;[13−18] note that III−Vs grown on III−V substrates have not yet been proven to be cost-effective for terrestrial applications. The recent resurgence of research on III−V/Si tandems[19−28] offers the promise of both long-term device stability and high efficiency, leveraging the vast PV knowledge base of both Si and III−V multijunction technologies. A III−V multijunction approach enables bandgap (E_g) tuning of each junction to more effectively utilize the entire solar spectrum. With a 1.6−1.8 eV top cell, III−V/Si tandems can achieve a theoretical efficiency of 37−44% under AM1.5G illumination, surpassing that of 1J Si devices by ∼10% absolute;[29,30] the range in theoretical efficiency stems from the difference in modeling assumptions used.

Direct, monolithic growth of III−Vs on Si allows for the use of large-area, low-cost Si substrates and a simplified integration

Received: June 23, 2017
Accepted: July 26, 2017
Published: July 26, 2017

DOI: 10.1021/acsenergylett.7b00538
ACS Energy Lett. 2017, 2, 1911−1918

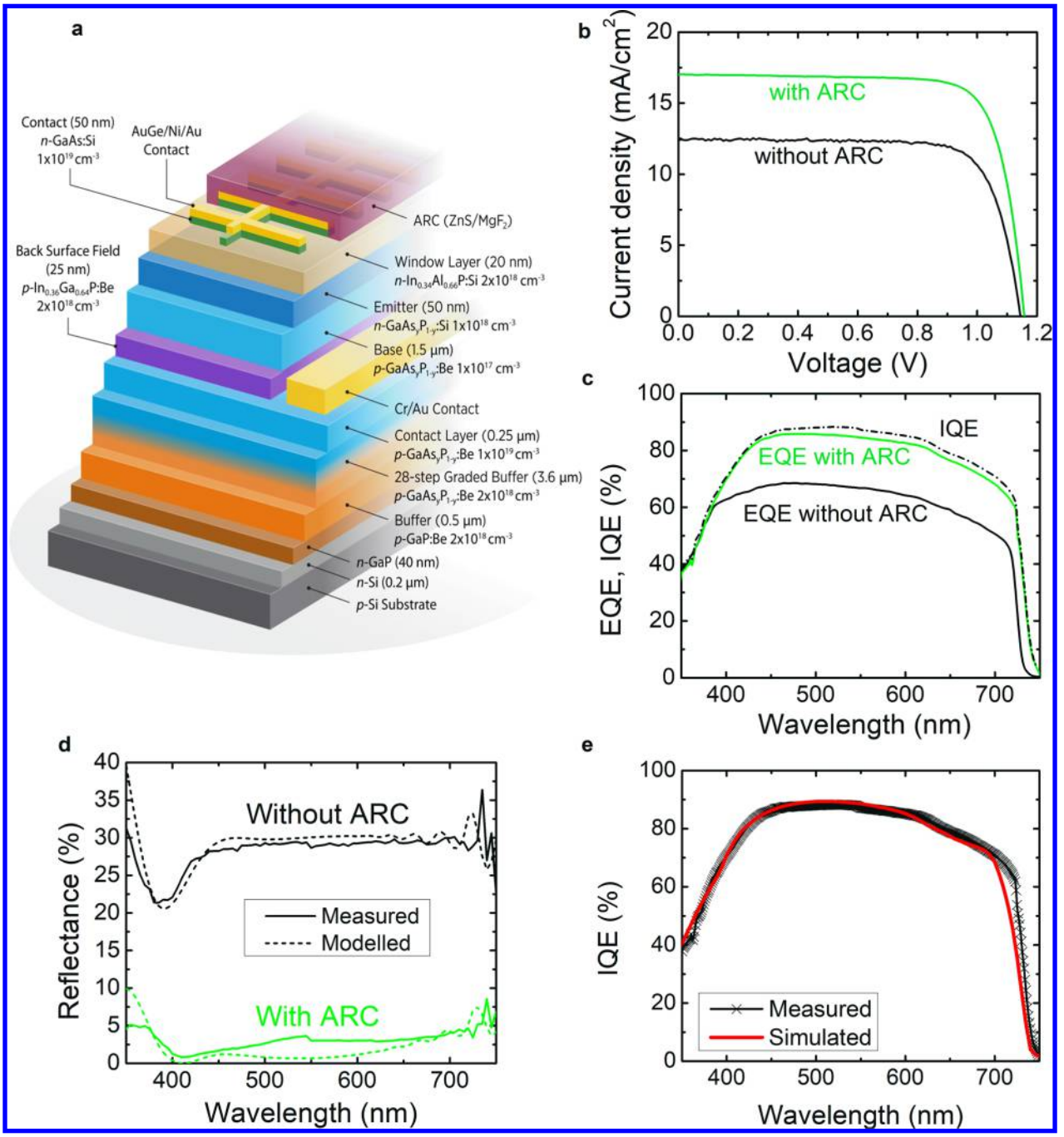

Figure 1. (a) Schematic of our 1J GaAsP solar cell on an inactive GaP/Si template. (b) LIV, (c) EQE (solid) and IQE (dot−dash), and (d) reflectance results for the 1J GaAsP/Si solar cell before (black) and after (green) ARC deposition. In (d), measured reflectance values (solid) are compared to modeled values (dashed) based on known optical constants for ARC materials and measured optical constants for nominally similar GaAsP and InAlP compositions. (e) Simulated (red) compared to measured (black) IQE of the record cell. The AR-coated LIV in (b) and EQE in (c) were certified by the National Renewable Energy Laboratory, and all other measurements were conducted in-house.

process and scale-up for modules, all of which can contribute toward reduced cost compared to wafer bonding and four-terminal designs.[31] As 1.6−1.8 eV III−V materials are all lattice-mismatched to Si, monolithic growth requires a metamorphic graded buffer to control the formation of mismatch-induced, performance-hindering dislocations; due to the ease of bandgap tuning with a metamorphic approach, even higher efficiency 3+ junction devices are also possible. $GaAs_yP_{1-y}$ is an ideal material for the top cell given its direct and tunable E_g in the range suitable for III−V/Si tandems. $GaAs_yP_{1-y}$ additionally benefits from the minimal lattice-mismatch between GaP and Si and the transparent compositional grading pathway from GaP to 1.7 eV $GaAs_yP_{1-y}$, enabling the use of GaP/Si as a growth template.

While direct growth of polar GaP on nonpolar Si is challenging, defect-free GaP on Si has been demonstrated in recent years.[32−36] This has enabled research into both 1J 1.7 eV $GaAs_yP_{1-y}$ top cells grown on GaP/Si templates as well as tandem devices utilizing an active Si bottom cell. Current state-of-the-art top cells lie between 6.9 and 12.0%[37−41] efficiency, whereas monolithic GaAsyP1-y/Si tandems are only slightly higher at 8.7−13.1%.[27,40] approximately 1/3 of the necessary efficiency for cost-competitive III−V/Si tandems.[31] The

DOI: 10.1021/acsenergylett.7b00538
ACS Energy Lett. 2017, 2, 1911−1918

Table 1. Device Parameters of the Hero 1J GaAsP/Si Solar Cell before and after ARC Deposition

	V_{oc} (V)	J_{sc} (mA/cm^2)	FF (%)	η (%)
without ARC (in-house)[a]	1.15	13.15	77.80	11.77
with ARC (in-house)[b]	1.16	18.03	78.49	16.42
with ARC (certified)[c]	1.1569 ± 0.2%	17.018 ± 2.2%	77.85 ± 0.4%	15.33 ± 2.2%

[a]Measured 3 weeks after initial growth. [b]Measured 17 months after initial growth. [c]Measured 5 months after initial growth. Uncertainties are relative and were reported by third-party certification.

$GaAs_yP_{1-y}$ top cell has impeded tandem performance and requires significant improvement to achieve the goal of low-cost, high-efficiency PV. In particular, these devices had short-circuit current densities (J_{SC}) less than ~13 mA/cm^2 and large bandgap−voltage offsets ($W_{OC} = E_g/q - V_{OC}$, where V_{OC} is the open-circuit voltage) of 0.55−0.70 V; realistic target values for J_{SC} and W_{OC} are 19−20 mA/cm^2 and 0.45−0.50 V, respectively, for 1J 1.7 eV GaAsP on Si solar cells.

In this work, we achieve a new, certified efficiency record for 1.7 eV 1J $GaAs_{0.76}P_{0.24}$ solar cells grown on GaP/Si templates (hereafter GaAsP/Si) of 15.3%, surpassing all previous work by a >25% relative margin.[37,41] We built upon our recent work on controlling nucleation and glide of threading dislocations throughout the $GaAs_yP_{1-y}$ graded buffer,[41] achieving a low threading dislocation density (TDD) of 5.3 × 10^6 cm^{-2}. Here, we developed an optimized antireflection coating (ARC) for 1J GaAsP/Si solar cells that reduced AM1.5G-weighted average reflectance from 28.7 down to 3.2%; this reduction in reflectance enhanced J_{SC} from 13.0 to 17.0 mA/cm^2 through an ~18% absolute improvement in external quantum efficiency (EQE) across all absorbed wavelengths. We discuss our results in the context of the field by comparing projected efficiencies of our cell in conjunction with state-of-the-art Si devices using the novel concept of spectral efficiency.[42] We show for the first time that GaAsP cells achieve sufficiently high performance to increase the power conversion efficiency when cascaded with state-of-the-art Si solar cells. To further illustrate the feasibility of achieving high tandem efficiency, we demonstrate a Si bottom cell with a GaAsP optical filter grown on top that attains an efficiency of 6.3%. Numerical simulations of our device results reveal realistic pathways toward enhancing the performance of future devices to achieve 20%-efficient top cells and 30% III−V/Si tandems,[31] a crucial step toward the commercialization of low-cost, high-efficiency PV.

Solar Cell Results. We grew the solar cell materials using molecular beam epitaxy (MBE) with a structure schematically represented in Figure 1a. In lattice-mismatched materials, such as those used in this work, threading dislocations are a primary contributor to nonradiative recombination. If not properly controlled, TDD can grow to values > 10^7 cm^{-2}, which can detrimentally affect V_{OC}.[43,44] As device TDD depends heavily on dislocation nucleation and glide kinetics, we recently investigated MBE growth conditions for the initial relaxed GaP buffer layer and $GaAs_yP_{1-y}$ graded buffer.[41] As a result of those studies, we discovered an optimal growth window that enables TDD values as low as 4.0 × 10^6 cm^{-2}. As can be seen in the device results in Figure 1b−d and Table 1, the as-grown, non-AR-coated solar cell achieved an efficiency of 11.77%, comparable to results that we published recently.[41]

Among J_{SC}, V_{OC}, and the fill factor (FF), J_{SC} offers the greatest potential for further improvements in efficiency, given that the J_{SC} of ~13.2 mA/cm^2 is over 40% less than the semiempirical limit of 22.5 mA/cm^2. To this end, we implemented an optimized ARC onto our device, which had not been done for previously published GaAsP/Si cells.[19,27,37−41,45] As the metamorphic materials used in this work are uncommon, we first characterized the refractive indices and extinction coefficients of individual layers of GaAsP and InAlP (Figure S1) using spectroscopic ellipsometry. We then designed an optimal dual-layer ARC of 29.4 nm ZnS/81.4 nm MgF_2 that reduced AM1.5G-weighted average reflectance from the bare cell from 28.7 down to just 3.2% in the relevant wavelength range of 350−750 nm (Figure 1d) for the top cell. Slight differences in the compositions of GaAsP and InAlP measured for optical constants from those in the device structure account for the minor differences in modeled versus measured reflectances in Figure 1d. Table 1 and Figure 1b illustrate the 1.3× improvement in J_{SC} due to the incorporation of this optimal ARC, along with a W_{OC} value of 0.525 V. The success of this ARC yielded improved EQE across wavelengths greater than 400 nm (Figure 1c), boosting efficiency to 15.33%; the shift in band edge seen in the EQE measured before and after ARC is believed to arise from a difference in wavelength calibration between the two different EQE systems with which these measurements were taken (in-house and certified at NREL). The lighted current−voltage (LIV) and EQE of our device with an ARC presented in Figure 1b,c and Table 1 was certified by the National Renewable Energy Laboratory.

We performed simulations using Silvaco TCAD Atlas to gain new insight into the relationship between TDD and device performance of GaAsP/Si solar cells. Emitter (L_p) and base (L_n) minority carrier diffusion lengths (lifetimes, τ) were found to be 52 nm (15 ps) and 1370 nm (400 ps), respectively (Figures 1e and S2 and Table 2). For comparison, the IQE data

Table 2. Simulated Base Minority Carrier Diffusion Lengths and Lifetimes (L_n, τ_n) and Measured TDD of Solar Cells Published in 2013,[38] 2014,[39] and in This Work

year	L_n (nm)	τ_n (ps)	TDD (cm^{-2})
2013	552	65	9.20 × 10^6
2014	631	85	7.78 × 10^6
this work	1370	400	5.25 × 10^6

of devices published in 2013[38] and 2014[39] were also simulated (Figure S3). The base L_n in this work greatly surpasses that of previous studies[38,39] by 2−3× due to the significant reduction in TDD. As is evident in Table 2, we have demonstrated significant progress in improving material quality, a fundamental challenge that has greatly hindered device performance in recent years.

To complement our top cell results, we developed a Si subcell that has undergone high-temperature III−V growth, utilizes GaP as a front-side electron contact, and is optically filtered by GaAsP, as would be the case in a realistic tandem architecture. The device was measured with a nonoptimized 110 nm SiN_x ARC (Figure 2) and attained an uncertified efficiency of 6.25% (~4−8% relative error), with J_{SC} = 19.5

DOI: 10.1021/acsenergylett.7b00538
ACS Energy Lett. 2017, 2, 1911−1918

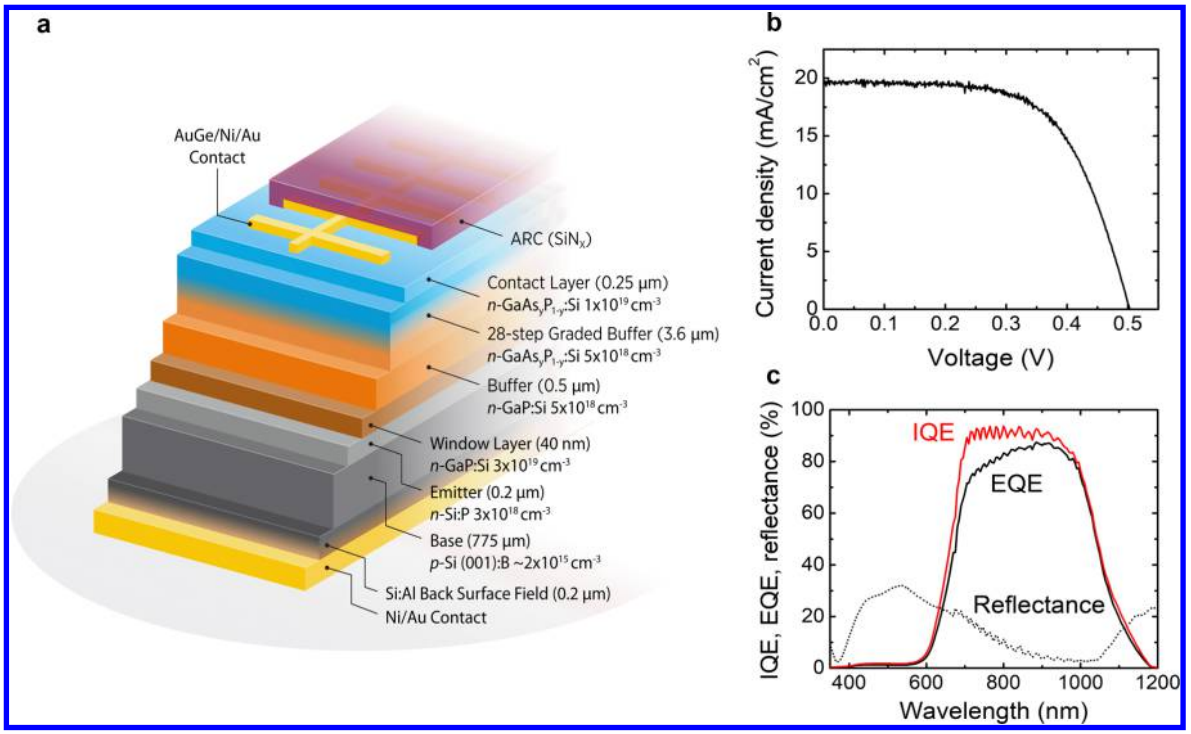

Figure 2. (a) Schematic of the 1J Si subcell grown on the same GaP/Si template as that used as a substrate for the certified GaAsP solar cell. This Si solar cell is optically filtered through an n-$GaAs_yP_{1-y}$ graded buffer meant to simulate the optical and growth conditions that would be experienced by a Si cell in a tandem architecture. (b) LIV and (c) IQE (red, solid), EQE (black, solid), and reflectance (black, dotted) results for the SiN_x-coated 1J Si solar cell.

mA/cm^2, V_{OC} = 0.503 V, and FF = 63.7%. The V_{OC} value is comparable to that in prior work on III−V-filtered Si bottom cells[27,40,46−48] and is indicative of degraded lifetimes from III−V growth;[49,50] while no wafer backside protection was employed in this work, protecting the backside of the Si prior to III−V growth could help mitigate lifetime degradation, as has been previously shown to enable V_{OC} values of up to 0.632 V.[26] The limited infrared response results from the nonoptimized wafer thickness (775 μm in this work compared to typical 180 μm-thick Si solar cells[51]) and lack of rear surface passivation[52,53] and could be improved upon in future work. The nonoptimized wafer thickness in conjunction with the low p-doping level in the Si substrate and concomitant high substrate resistivity of 8−12 Ω−cm (compared to typical 1−2 Ω−cm in diffused Si solar cells[51]) likely contributes to the large series resistance in our device; while it has not yet been investigated, the GaP electron contact could potentially impact device series resistance, as well. Given that the GaAsP optical filter layer utilized on this cell is thinner than would be used in a tandem architecture, the Si bottom cell EQE would be reduced between 600 and 730 nm in a tandem due to absorption in the top cell with concomitant reductions in J_{SC} and efficiency. The combination of this optically filtered Si bottom cell with our best GaAsP top cell has the potential to achieve a four-terminal tandem efficiency of 19.9−22.3%, where higher values can be approached with an excellent broad-band ARC, as calculated using spectral efficiency (see the calculation description in the Supporting Information).[42]

Perspective on State-of-the-Art III−V/Si Tandems. The current best monolithic tandem GaAsP/Si device has an efficiency of 13.1%,[27] while our top cell alone is 2% absolute higher. In order to realistically project the potential impact of our GaAsP cell in a Si-based tandem, we employ the recently proposed empirical construct of spectral efficiency.[42] Spectral efficiency is defined as the power conversion efficiency of a solar cell resolved by wavelength. This spectrum is calculated using a solar cell's V_{OC}, FF, and $J_{SC}(\lambda)$, the latter of which is a function of the EQE(λ) or internal quantum efficiency [IQE(λ)] and spectral irradiance;[42] EQE- and IQE-based spectral efficiencies shall hereafter be referred to as external and internal spectral efficiency (ESE and ISE). A proposed tandem device's maximum power conversion efficiency for any combination of subcells can be computed by summing the integrated subcells' spectral efficiencies, weighted by the fraction of light at each wavelength that reaches each subcell (see the Supporting Information).[42] In order for a Si-based tandem to achieve higher efficiency than a Si cell alone, the spectral efficiency of the top cell must exceed that of Si for photons with energy > $E_{g,top\ cell}$. The strength of the spectral efficiency concept is that it allows one to unambiguously determine if integrating a given top cell with Si is worthwhile. In addition, for a given top cell, the potential tandem efficiency can be estimated for a range of Si bottom cell technologies.

In Figure 3, we plot the ISE and ESE of our record GaAsP top cell, our recently published uncoated GaAsP cell,[41] Geisz's past 9.8% record GaAsP cell,[37] and the current best Si cell that has undergone III−V growth.[26] As ISE eliminates the effects of reflection and thus allows for comparisons between devices with and without ARCs, the significant improvement in material quality and device performance in our cell becomes quite evident when comparing Geisz's and our cell's ISEs. Another key attribute of this figure is that our GaAsP cell's ISE lies far above that of Feifel's Si cell for wavelengths lower than our top cell bandgap. This additionally holds true when comparing our GaAsP ESE with that of one of the best monocrystalline Si cells[54] (not shown); our device's ESE

DOI: 10.1021/acsenergylett.7b00538
ACS Energy Lett. 2017, 2, 1911−1918

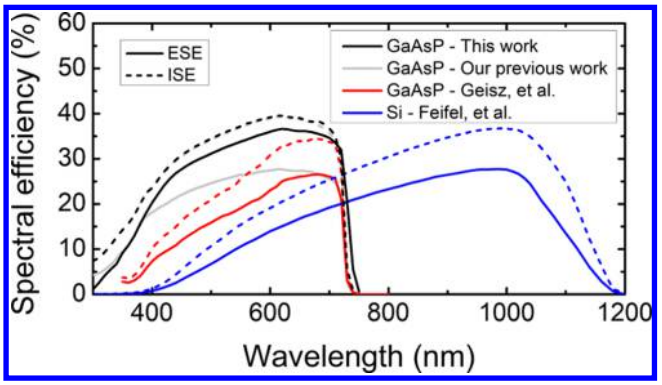

Figure 3. Internal (dashed) and external (solid) spectral efficiency (ISE and ESE, respectively) of this work (black) compared to our past work[41] (gray), Geisz's cell[37] (red), and the best Si cell that has undergone III−V growth[26] (blue).

exceeds that of previous record 1J Si cells by ≳7% absolute in the range of 400−700 nm. From this, we can conclude that our GaAsP cell is capable of providing a substantial efficiency contribution beyond that of 1J Si devices.

This point is further illustrated in Table 3. On the basis of the current state-of-the-art, if we were to form a four-terminal tandem out of our record GaAsP cell reported here and one of the best reported monocrystalline Si devices,[54] this tandem would achieve a maximum of ∼27% efficiency. While it is encouraging that we would be just 3% (absolute) below the target tandem efficiency of 30%, this result is overly optimistic; given the monolithic approach, the underlying Si would utilize different front-surface passivation than this record cell, would face the challenge of III−V epitaxy-induced lifetime degradation,[49,50] and would furthermore need to employ back surface passivation fabrication techniques compatible with the upper III−V layers.[53] To this end, we calculated the projected tandem efficiency for our GaAsP cell with Feifel's result,[26] which is the best-in-class Si cell that underwent III−V growth and utilized GaP for front-surface passivation,[46,50,55−58] as would occur in a monolithic GaAsP/Si tandem. Such a tandem would achieve a more realistic maximum efficiency of 22.2−25.6%, where the higher values can be approached with an excellent ARC (Table 3).

Toward a 30% III−V/Si Tandem. Leveraging the results presented here, we performed additional simulations to better understand the underlying limitations in these solar cells and to determine a realistic pathway toward the target 20% top cell and 30% III−V/Si tandem. For the current material lifetimes, simulations showed our device design to be close to optimal in terms of layer thicknesses (Figures S4−S6). The front metal grid coverage was identified as one of the primary contributors to current and efficiency losses. By reducing grid coverage from 8 to 1% and adjusting the grid geometry to be similar to that of record devices,[59,60] we can enhance J_{SC}, V_{OC}, and FF to 18.3 mA/cm^2, 1.16 V, and 79.7%, respectively. This would improve top cell efficiency to 16.93% in the near-term (Figure 4) without requiring any significant improvements in material quality.

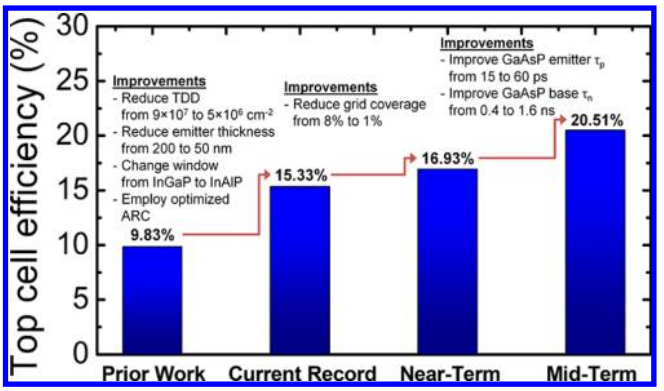

Figure 4. Realistic pathway toward a target 20%-efficient top cell for a 30% III−V/Si tandem.

In order to improve top cell efficiency toward 20%, the active region material quality must be improved, as we previously accomplished last year with a ∼2× reduction in TDD.[41] We could realistically improve the GaAsP base lifetime τ_n by 4× to ∼1.6 ns through a combination of reducing TDD[61] down to ∼1 × 10^6 cm^{-2} and postgrowth annealing;[62,63] note that in earlier work,[61] τ_n = 1.54 ns was attained for *p*-GaAs on SiGe/Si for samples with TDD ≈ 1 × 10^6 cm^{-2}. With an increased τ_n in conjunction with a 4× improvement in emitter lifetime τ_p and an optimal emitter (base) thickness of 30 nm (2.3 μm), we simulate a J_{SC}, V_{OC}, and FF of 20.3 mA/cm^2, 1.23 V, and 82.2%, respectively. This simulated efficiency improvement up to 20.51% achieves the top cell target efficiency (Figures 4 and S7). With the implementation of a high-performance broadband ARC (Figure S8), we anticipate that a ∼10% bottom cell contribution can be realistically achieved, based on the 9.9% contribution of Feifel's Si subcell in the ISE-based tandem efficiency calculation (Table 3). Given this 10% bottom cell efficiency, along with the proposed enhancements to our GaAsP top cell to reach 20% efficiency, we believe that this Letter paves the way for a monolithic 30% GaAsP/Si tandem. In parallel to the above improvements, future research should also focus on demonstrating high-efficiency cells with larger areas.

Through the implementation of an optimized ARC in conjunction with our recent developments in material quality and device design, we have achieved a certified 15.3%-efficient 1J GaAsP/Si solar cell. Our work greatly surpasses all previous records, demonstrating significant progress toward a high-

Table 3. Projected Tandem Efficiencies of Various GaAsP Top Cells with Feifel's Si Subcell and Their Respective Efficiency Contributions Based on Internal and External Spectral Efficiency

		projected tandem efficiency with Feifel's Si (%)		ESE subcell efficiency contribution (%)		ISE subcell efficiency contribution (%)	
GaAsP top cell	fraction of detailed balance efficiency (%)	ESE	ISE	GaAsP	Si	GaAsP	Si
Geisz et al.[37]	34.1	17.01	21.60	9.78	7.23	11.97	9.63
our recent work in 2016[41]	40.2	18.95	25.58	11.51	7.44	15.68	9.90
this work	52.3	22.24	25.58	15.01	7.23	15.68	9.90

DOI: 10.1021/acsenergylett.7b00538
ACS Energy Lett. 2017, 2, 1911−1918

efficiency, cost-competitive III−V/Si tandem. As expected, our devices are stable, having been certified after 5 months of storage in ambient conditions following device growth and remeasured with comparable performance ∼1.5 years after growth (Table 1). In addition, we demonstrated an unoptimized Si bottom cell that we expect to deliver at least 4.6% additional efficiency in a tandem configuration. Using the novel construct of spectral efficiency, we project that our device in tandem with the best Si subcell that has undergone III−V growth could achieve 25.6% efficiency, nearly double that of current GaAsP/Si tandems. Using the cell reported here as a starting point, simulations outline a realistic pathway toward 20% top cell efficiency. Through optimization of the top metal grid, followed by feasible enhancements to GaAsP material quality in conjunction with a 10% bottom Si cell, a monolithic 30% GaAsP/Si tandem can be achieved.

■ ASSOCIATED CONTENT

Supporting Information

The Supporting Information is available free of charge on the ACS Publications website at DOI: 10.1021/acsenergylett.7b00538.

Measured GaAsP and InAlP optical coefficients, spectral efficiency calculation information, additional *IV* and QE simulations of GaAsP top cells, further discussion of ARCs for GaAsP/Si tandems, and experimental methods (PDF)

■ AUTHOR INFORMATION

Corresponding Author

*E-mail: mllee@illinois.edu.

ORCID

Michelle Vaisman: 0000-0001-6456-7450

Notes

The authors declare no competing financial interest.

■ ACKNOWLEDGMENTS

Funding for this work was provided by NSF Awards 1736181, 1509687, and 1509864. Yale Institute for Nanoscience and Quantum Engineering MRSEC facilities used in this work were supported under DMR-1119826. M.V. was supported by a National Aeronautics and Space Administration (NASA) Space Technology Research Fellowship. K.N.Y. was supported by a National Research Foundation graduate research fellowship provided by the Singapore Energy Innovation Programme Office. D.M.-M. acknowledges support from the Spanish Ministerio de Economía y Competitividad under Project TEC2015-66722-R and Comunidad de Madrid under Project SINFOTON S2013/MIT-2790. We gratefully acknowledge the assistance of Tom Moriarty at the National Renewable Energy Laboratory in certifying our GaAsP solar cells. Research on the Si bottom cell was carried out in part in the Micro and Nanotechnology Laboratory and Frederick Seitz Materials Research Laboratory Central Research Facilities at the University of Illinois.

■ REFERENCES

(1) *The SunShot Initiative's 2030 Goal: 3¢ per Kilowatt Hour for Solar Electricity*; Report DOE/EE-1501; U.S. Department of Energy, 2016.

(2) Yoshikawa, K.; Kawasaki, H.; Yoshida, W.; Irie, T.; Konishi, K.; Nakano, K.; Uto, T.; Adachi, D.; Kanematsu, M.; Uzu, H.; et al. Silicon Heterojunction Solar Cell with Interdigitated Back Contacts for a Photoconversion Efficiency over 26%. *Nat. Energy* **2017**, *2*, 17032.

(3) Richter, A.; Hermle, M.; Glunz, S. W. Reassessment of the Limiting Efficiency for Crystalline Silicon Solar Cells. *IEEE J. Photovolt.* **2013**, *3*, 1184−1191.

(4) McMeekin, D. P.; Sadoughi, G.; Rehman, W.; Eperon, G. E.; Saliba, M.; Hörantner, M. T.; Haghighirad, A.; Sakai, N.; Korte, L.; Rech, B.; et al. A Mixed-Cation Lead Mixed-Halide Perovskite Absorber for Tandem Solar Cells. *Science* **2016**, *351*, 151−155.

(5) Bailie, C. D.; Christoforo, M. G.; Mailoa, J. P.; Bowring, A. R.; Unger, E. L.; Nguyen, W. H.; Burschka, J.; Pellet, N.; Lee, J. Z.; Grätzel, M.; et al. Semitransparent Perovskite Solar Cells for Tandems with Silicon and CIGS. *Energy Environ. Sci.* **2015**, *8*, 956−963.

(6) Albrecht, S.; Saliba, M.; Correa Baena, J. P.; Lang, F.; Kegelmann, L.; Mews, M.; Steier, L.; Abate, A.; Rappich, J.; Korte, L.; et al. Monolithic Perovskite/Silicon-Heterojunction Tandem Solar Cells Processed at Low Temperature. *Energy Environ. Sci.* **2016**, *9*, 81−88.

(7) Bush, K. A.; Palmstrom, A. F.; Yu, Z. J.; Boccard, M.; Cheacharoen, R.; Mailoa, J. P.; McMeekin, D. P.; Hoye, R. L. Z.; Bailie, C. D.; Leijtens, T.; et al. 23.6%-Efficient Monolithic Perovskite/Silicon Tandem Solar Cells with Improved Stability. *Nat. Energy* **2017**, *2*, 17009.

(8) Werner, J.; Barraud, L.; Walter, A.; Bräuninger, M.; Sahli, F.; Sacchetto, D.; Tétreault, N.; Paviet-Salomon, B.; Moon, S.-J.; Allebé, C.; et al. Efficient Near-Infrared-Transparent Perovskite Solar Cells Enabling Direct Comparison of 4-Terminal and Monolithic Perovskite/Silicon Tandem Cells. *ACS Energy Lett.* **2016**, *1*, 474−480.

(9) Chen, B.; Bai, Y.; Yu, Z.; Li, T.; Zheng, X.; Dong, Q.; Shen, L.; Boccard, M.; Gruverman, A.; Holman, Z.; et al. Efficient Semitransparent Perovskite Solar Cells for 23.0%-Efficiency Perovskite/Silicon Four-Terminal Tandem Cells. *Adv. Energy Mater.* **2016**, *6*, 1601128.

(10) Duong, T.; Wu, Y.; Shen, H.; Peng, J.; Fu, X.; Jacobs, D.; Wang, E.-C.; Kho, T. C.; Fong, K. C.; Stocks, M.; et al. Rubidium Multication Perovskite with Optimized Bandgap for Perovskite-Silicon Tandem with over 26% Efficiency. *Adv. Energy Mater.* **2017**, *7*, 1700228.

(11) Mailoa, J. P.; Bailie, C. D.; Johlin, E. C.; Hoke, E. T.; Akey, A. J.; Nguyen, W. H.; McGehee, M. D.; Buonassisi, T. A 2-Terminal Perovskite/Silicon Multijunction Solar Cell Enabled by a Silicon Tunnel Junction. *Appl. Phys. Lett.* **2015**, *106*, 121105.

(12) Werner, J.; Walter, A.; Rucavado, E.; Moon, S.-J.; Sacchetto, D.; Rienaecker, M.; Peibst, R.; Brendel, R.; Niquille, X.; De Wolf, S.; et al. Zinc Tin Oxide as High-Temperature Stable Recombination Layer for Mesoscopic Perovskite/Silicon Monolithic Tandem Solar Cells. *Appl. Phys. Lett.* **2016**, *109*, 233902.

(13) Algora, C. Reliability of III−V Concentrator Solar Cells. *Microelectron. Reliab.* **2010**, *50*, 1193−1198.

(14) Strevel, N.; Trippel, L.; Kotarba, C.; Khan, I. Improvements in CdTe Module Reliability and Long-Term Degradation through Advances in Construction and Device Innovation. *Photovoltaics International* **2014**, 22.

(15) Branker, K.; Pathak, M. J. M.; Pearce, J. M. A Review of Solar Photovoltaic Levelized Cost of Electricity. *Renewable Sustainable Energy Rev.* **2011**, *15*, 4470−4482.

(16) Hardikar, K.; Vitkavage, D.; Saproo, A.; Krajewski, T. *Predicting Edge Seal Performance From Accelerated Testing*; Proc. SPIE: San Diego, CA, 2014; p 91790N.

(17) Coyle, D. J. Life Prediction for CIGS Solar Modules Part 1: Modeling Moisture Ingress and Degradation. *Prog. Photovoltaics* **2013**, *21*, 156−172.

(18) Coyle, D. J.; Blaydes, H. A.; Northey, R. S.; Pickett, J. E.; Nagarkar, K. R.; Zhao, R.-A.; Gardner, J. O. Life Prediction for CIGS Solar Modules Part 2: Degradation Kinetics, Accelerated Testing, and Encapsulant Effects. *Prog. Photovoltaics* **2013**, *21*, 173−186.

(19) Grassman, T. J.; Brenner, M. R.; Gonzalez, M.; Carlin, A. M.; Unocic, R. R.; Dehoff, R. R.; Mills, M. J.; Ringel, S. A. Characterization of Metamorphic GaAsP/Si Materials and Devices for Photovoltaic Applications. *IEEE Trans. Electron Devices* **2010**, *57*, 3361−3369.

DOI: 10.1021/acsenergylett.7b00538
ACS Energy Lett. 2017, 2, 1911−1918

(20) Holm, J. V.; Jørgensen, H. I.; Krogstrup, P.; Nygård, J.; Liu, H.; Aagesen, M. Surface-Passivated GaAsP Single-Nanowire Solar Cells Exceeding 10% Efficiency Grown on Silicon. *Nat. Commun.* **2013**, *4*, 1498.
(21) Dimroth, F.; Roesener, T.; Essig, S.; Weuffen, C.; Wekkeli, A.; Oliva, E.; Siefer, G.; Volz, K.; Hannappel, T.; Häussler, D.; et al. Comparison of Direct Growth and Wafer Bonding for the Fabrication of GaInP/GaAs Dual-Junction Solar Cells on Silicon. *IEEE J. Photovolt.* **2014**, *4*, 620−625.
(22) Chmielewski, D.; Grassman, T. J.; Carlin, A. M.; Carlin, J. A.; Speelman, A. J.; Ringel, S. A. Metamorphic GaAsP Tunnel Junctions for High-Efficiency III−V/IV Multijunction Solar Cell Technology. *IEEE J. Photovolt.* **2014**, *4*, 1301−1305.
(23) Tamboli, A. C.; van Hest, M. F. A. M.; Steiner, M. A.; Essig, S.; Perl, E. E.; Norman, A. G.; Bosco, N.; Stradins, P. III-V/Si Wafer Bonding Using Transparent, Conductive Oxide Interlayers. *Appl. Phys. Lett.* **2015**, *106*, 263904.
(24) Essig, S.; Benick, J.; Schachtner, M.; Wekkeli, A.; Hermle, M.; Dimroth, F. Wafer-bonded GaInP/GaAs//Si Solar Cells with 30% Efficiency Under Concentrated Sunlight. *IEEE J. Photovolt.* **2015**, *5*, 977−981.
(25) Essig, S.; Steiner, M. A.; Allebé, C.; Geisz, J. F.; Paviet-Salomon, B.; Ward, S.; Descoeudres, A.; LaSalvia, V.; Barraud, L.; Badel, N.; et al. Realization of GaInP/Si Dual-Junction Solar Cells with 29.8% 1-Sun Efficiency. *IEEE J. Photovolt.* **2016**, *6*, 1012−1019.
(26) Feifel, M.; Rachow, T.; Benick, J.; Ohlmann, J.; Janz, S.; Hermle, M.; Dimroth, F.; Lackner, D. Gallium Phosphide Window Layer for Silicon Solar Cells. *IEEE J. Photovolt.* **2016**, *6*, 384−390.
(27) Grassman, T. J.; Chmielewski, D. J.; Carnevale, S. D.; Carlin, J. A.; Ringel, S. A. $GaAs_{0.75}P_{0.25}$/Si Dual-Junction Solar Cells Grown by MBE and MOCVD. *IEEE J. Photovolt.* **2016**, *6*, 326−331.
(28) Cariou, R.; Benick, J.; Beutel, P.; Razek, N.; Flötgen, C.; Hermle, M.; Lackner, D.; Glunz, S. W.; Bett, A. W.; Wimplinger, M.; et al. Monolithic Two-Terminal III-V//Si Triple-Junction Solar Cells with 30.2% Efficiency Under 1-Sun AM1.5g. *IEEE J. Photovolt.* **2017**, *7*, 367−373.
(29) Geisz, J. F.; Friedman, D. J. III−N−V Semiconductors for Solar Photovoltaic Applications. *Semicond. Sci. Technol.* **2002**, *17*, 769.
(30) Grassman, T. J.; Carlin, A. M.; Grandal, J.; Ratcliff, C.; Yang, L.; Mills, M. J.; Ringel, S. A. Spectrum-Optimized Si-based III-V Multijunction Photovoltaics. *Proc. SPIE* **2012**, 8256.
(31) Woodhouse, M.; Goodrich, A. *A Manufacturing Cost Analysis Relevant to Single- and Dual-Junction Photovoltaic Cells Fabricated with III−Vs and III−Vs Grown on Czochralski Silicon*; National Renewable Energy Laboratory Report No. PR-6A20-60126; 2013.
(32) Grassman, T.; Brenner, M. R.; Rajagopalan, S.; Unocic, R.; Dehoff, R.; Mills, M.; Fraser, H.; Ringel, S. A. Control and Elimination of Nucleation-Related Defects in GaP/Si(001) Heteroepitaxy. *Appl. Phys. Lett.* **2009**, *94*, 232106.
(33) Volz, K.; Beyer, A.; Witte, W.; Ohlmann, J.; Németh, I.; Kunert, B.; Stolz, W. GaP-Nucleation on Exact Si (001) Substrates for III/V Device Integration. *J. Cryst. Growth* **2011**, *315*, 37−47.
(34) Grassman, T. J.; Carlin, J. A.; Galiana, B.; Yang, L.-M.; Yang, F.; Mills, M. J.; Ringel, S. A. Nucleation-Related Defect-Free GaP/Si(100) Heteroepitaxy via Metal-Organic Chemical Vapor Deposition. *Appl. Phys. Lett.* **2013**, *102*, 142102.
(35) Warren, E. L.; Kibbler, A. E.; France, R. M.; Norman, A. G.; Stradins, P.; McMahon, W. E. Growth of Antiphase-Domain-Free GaP on Si Substrates by Metalorganic Chemical Vapor Deposition Using an In Situ AsH_3 Surface Preparation. *Appl. Phys. Lett.* **2015**, *107*, 082109.
(36) Supplie, O.; May, M. M.; Kleinschmidt, P.; Nägelein, A.; Paszuk, A.; Brückner, S.; Hannappel, T. In Situ Controlled Heteroepitaxy of Single-Domain GaP on As-Modified Si(100). *APL Mater.* **2015**, *3*, 126110.
(37) Geisz, J. F.; Olson, J. M.; Romero, M. J.; Jiang, C. S.; Norman, A. G. *Lattice-Mismatched GaAsP Solar Cells Grown on Silicon by OMVPE*, Conf. Rec. IEEE 4th World Conf. Photovolt. Energy Convers., Waikoloa, Hawaii, 2006; pp 772−775.
(38) Lang, J. R.; Faucher, J.; Tomasulo, S.; Nay Yaung, K.; Lee, M. L. Comparison of GaAsP Solar Cells on GaP and GaP/Si. *Appl. Phys. Lett.* **2013**, *103*, 092102.
(39) Nay Yaung, K.; Lang, J. R.; Lee, M. L. *Towards High Efficiency GaAsP Solar Cells on (001) GaP/Si*, Proc. 40th IEEE Photovolt. Spec. Conf., Denver, CO, 2014; pp 0831−0835.
(40) Grassman, T. J.; Carlin, J. A.; Ratcliff, C.; Chmielewski, D. J.; Ringel, S. A. *Epitaxially-Grown Metamorphic GaAsP/Si Dual-Junction Solar Cells*, Proc. 39th IEEE Photovolt. Spec. Conf., Tampa, FL, 2013; pp 0149−0153.
(41) Nay Yaung, K.; Vaisman, M.; Lang, J.; Lee, M. L. GaAsP Solar Cells on GaP/Si with Low Threading Dislocation Density. *Appl. Phys. Lett.* **2016**, *109*, 032107.
(42) Yu, Z.; Leilaeioun, M.; Holman, Z. Selecting Tandem Partners for Silicon Solar Cells. *Nat. Energy* **2016**, *1*, 16137.
(43) Yamaguchi, M.; Amano, C. Efficiency Calculations of Thin-Film GaAs Solar Cells on Si Substrates. *J. Appl. Phys.* **1985**, *58*, 3601−3606.
(44) Andre, C. L.; Wilt, D. M.; Pitera, A. J.; Lee, M. L.; Fitzgerald, E. A.; Ringel, S. A. Impact of Dislocation Densities on n^+/p and p^+/n Junction GaAs Diodes and Solar Cells on SiGe Virtual Substrates. *J. Appl. Phys.* **2005**, *98*, 014502.
(45) Vaisman, M.; Nay Yaung, K.; Sun, Y.; Lee, M. L. *GaAsP/Si Solar Cells and Tunnel Junctions for III-V/Si Tandem Devices*, Proc. 43rd IEEE Photovolt. Spec. Conf.; IEEE: Portland, OR, 2016; pp 2043−2047.
(46) Grassman, T. J.; Carlin, J. A.; Galiana, B.; Yang, F.; Mills, M. J.; Ringel, S. A. MOCVD-Grown GaP/Si Subcells for Integrated III-V/Si Multijunction Photovoltaics. *IEEE J. Photovolt.* **2014**, *4*, 972−980.
(47) Geisz, J. F.; Olson, J. M.; Friedman, D. J.; Jones, K. M.; Reedy, R. C.; Romero, M. J. *Lattice-Matched GaNPAs-on-Silicon Tandem Solar Cells*, Proc. 31st IEEE Photovolt. Spec. Conf., Lake Buena Vista, FL, 2005; pp 695−698.
(48) Ringel, S. A.; Carlin, J. A.; Grassman, T. J.; Galiana, B.; Carlin, A. M.; Ratcliff, C.; Chmielewski, D.; Yang, L.; Mills, M. J.; Mansouri, A.; et al. *Ideal GaP/Si Heterostructures Grown by MOCVD: III−V/Active-Si Subcells, Multijuntions, and MBE-to-MOCVD III−V/Si Interface Science*, Proc. 39th IEEE Photovolt. Spec. Conf., Tampa, FL, 2013; pp 3383−3388.
(49) Ding, L.; Zhang, C.; Nærland, T. U.; Faleev, N.; Honsberg, C.; Bertoni, M. I. Silicon Minority-Carrier Lifetime Degradation During Molecular Beam Heteroepitaxial III-V Material Growth. *Energy Procedia* **2016**, *92*, 617−623.
(50) García-Tabarés, E.; Rey-Stolle, I. Impact of Metal-Organic Vapor Phase Epitaxy Environment on Silicon Bulk Lifetime for III−V-on-Si Multijunction Solar Cells. *Sol. Energy Mater. Sol. Cells* **2014**, *124*, 17−23.
(51) Aberle, A. G. Surface Passivation of Crystalline Silicon Solar Cells: A Review. *Prog. Photovoltaics* **2000**, *8*, 473−487.
(52) Green, M. A. *Solar Cells: Operating Principles, Technology, and System Applications*; The University of New South Wales: Kensington, New South Wales, 1998.
(53) Martín-Martín, D.; García-Tabarés, E.; Rey-Stolle, I. Assessment of Rear-Surface Processing Strategies for III-V on Si Multijunction Solar Cells Based on Numerical Simulations. *IEEE Trans. Electron Devices* **2016**, *63*, 252−258.
(54) Green, M. A.; Emery, K.; Hishikawa, Y.; Warta, W.; Dunlop, E. D. Solar Cell Efficiency Tables (Version 48). *Prog. Photovoltaics* **2016**, *24*, 905−913.
(55) Varache, R.; Darnon, M.; Descazeaux, M.; Martin, M.; Baron, T.; Muñoz, D. Evolution of Bulk c-Si Properties During the Processing of GaP/c-Si Heterojunction Cell. *Energy Procedia* **2015**, *77*, 493−499.
(56) Almansouri, I.; Bremner, S.; Ho-Baillie, A.; Mehrvarz, H.; Hao, X.; Conibeer, G.; Grassman, T. J.; Carlin, J. A.; Haas, A.; Ringel, S. A.; et al. Designing Bottom Silicon Solar Cells for Multijunction Devices. *IEEE J. Photovolt.* **2015**, *5*, 683−690.
(57) García-Tabarés, E.; García, I.; Lelièvre, J.-F.; Rey-Stolle, I. Impact of a Metal−Organic Vapor Phase Epitaxy Environment on Silicon Substrates for III−V-on-Si Multijunction Solar Cells. *Jpn. J. Appl. Phys.* **2012**, *51*, 10ND05.

DOI: 10.1021/acsenergylett.7b00538
ACS Energy Lett. 2017, 2, 1911−1918

(58) Zhang, C.; Faleev, N. N.; Ding, L.; Boccard, M.; Bertoni, M.; Holman, Z.; King, R. R.; Honsberg, C. B. *Hetero-Emitter GaP/Si Solar Cells with High Si Bulk Lifetime*, Proc. 43rd IEEE Photovolt. Spec. Conf., Portland, OR, 2016; pp 1950−1953.
(59) Bauhuis, G. J.; Mulder, P.; Haverkamp, E. J.; Huijben, J. C. C. M.; Schermer, J. J. 26.1% Thin-Film GaAs Solar Cell Using Epitaxial Lift-off. *Sol. Energy Mater. Sol. Cells* **2009**, *93*, 1488−1491.
(60) Steiner, M. A.; Geisz, J. F.; García, I.; Friedman, D. J.; Duda, A.; Kurtz, S. R. Optical Enhancement of the Open-Circuit Voltage in High Quality GaAs Solar Cells. *J. Appl. Phys.* **2013**, *113*, 123109.
(61) Andre, C. L.; Boeckl, J. J.; Wilt, D. M.; Pitera, A. J.; Lee, M. L.; Fitzgerald, E. A.; Keyes, B. M.; Ringel, S. A. Impact of Dislocations on Minority Carrier Electron and Hole Lifetimes in GaAs Grown on Metamorphic SiGe Substrates. *Appl. Phys. Lett.* **2004**, *84*, 3447−3449.
(62) Faucher, J.; Sun, Y.; Jung, D.; Martin, D.; Masuda, T.; Lee, M. L. High-Efficiency AlGaInP Solar Cells Grown by Molecular Beam Epitaxy. *Appl. Phys. Lett.* **2016**, *109*, 172105.
(63) Kurtz, S. R.; Allerman, A. A.; Jones, E. D.; Gee, J. M.; Banas, J. J.; Hammons, B. E. InGaAsN Solar Cells with 1.0 eV Band Gap, Lattice Matched to GaAs. *Appl. Phys. Lett.* **1999**, *74*, 729−731.

DOI: 10.1021/acsenergylett.7b00538
ACS Energy Lett. 2017, 2, 1911−1918

Supporting Information

15.3%-Efficient GaAsP Solar Cells on GaP/Si Templates

Michelle Vaisman[1,2], Shizhao Fan[3], Kevin Nay Yaung[1], Emmett Perl[2], Diego Martín-Martín[4], Zhengshan J. Yu[5], Mehdi Leilaeioun[5], Zachary C. Holman[5] and Minjoo L. Lee[3]*

[1]Department of Electrical Engineering, Yale University, New Haven, Connecticut 06511, USA.

[2]National Renewable Energy Laboratory, Golden, Colorado 80401, USA.

[3]Department of Electrical and Computer Engineering, University of Illinois Urbana-Champaign, Urbana, Illinois 61801, USA.

[4]Área de Tecnología Electrónica, Universidad Rey Juan Carlos, Móstoles, Madrid 28933, Spain.

[5]School of Electrical, Computer and Energy Engineering, Arizona State University, Tempe, Arizona 85287, USA.

*e-mail: mllee@illinois.edu

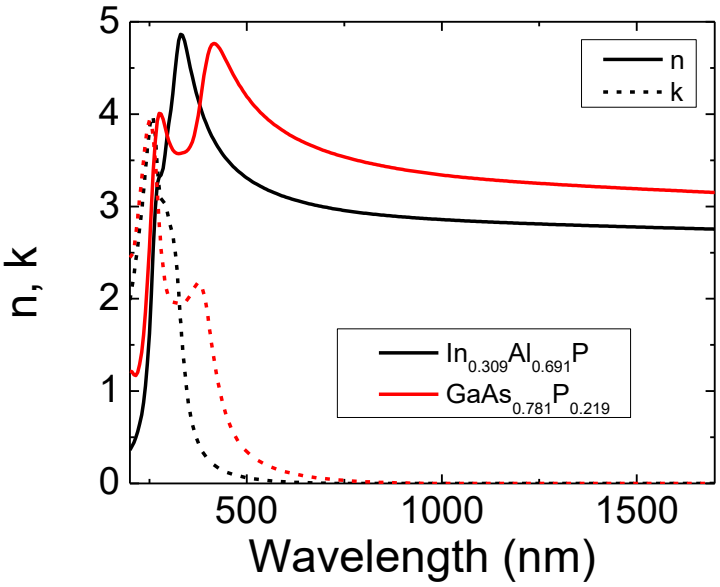

Figure S1. Measured n and k optical coefficients for InAlP and GaAsP. Optical coefficients for slightly different compositions of InAlP and GaAsP were reported by Conrad, et al.[1]

Spectral Efficiency Calculations. In calculating tandem efficiencies from spectral efficiency, one must assume a particular spectral fidelity for each cell, which is defined as the fraction of incident light that reaches a given subcell as a function of wavelength. For simplicity of calculation, in this work, we do not apply the constraint of tandem current limiting, but instead assume that a beam splitter couples both cells in a four-terminal configuration, as described elsewhere.[2] In the calculation of projected tandem efficiencies in Table 3, EQEs of both top and bottom subcells were used for the "ESE" column, and IQEs of both subcells were used for the "ISE" column. EQE and IQE data of all previously published devices for spectral efficiency calculations were digitized from their respective references.

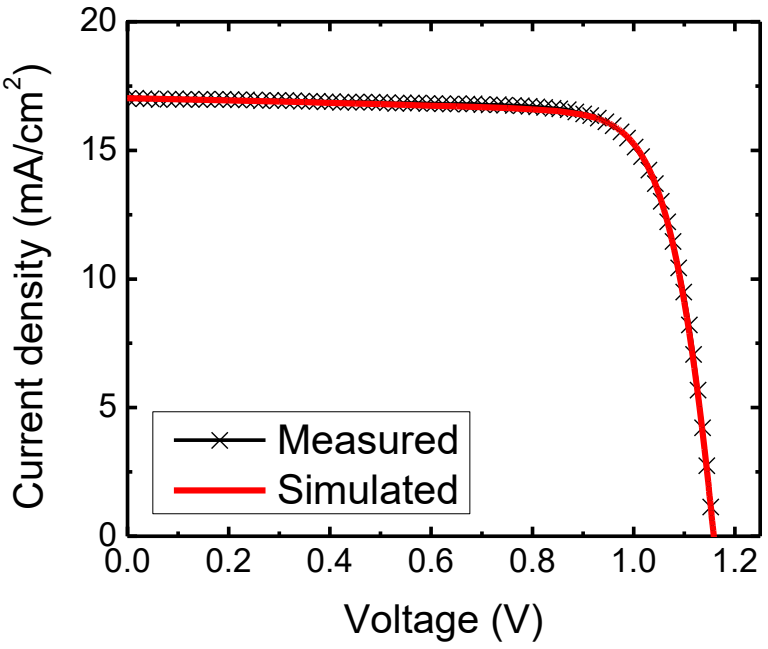

Figure S2. Simulation (red) compared to measured (black crosses) LIV of our record cell.

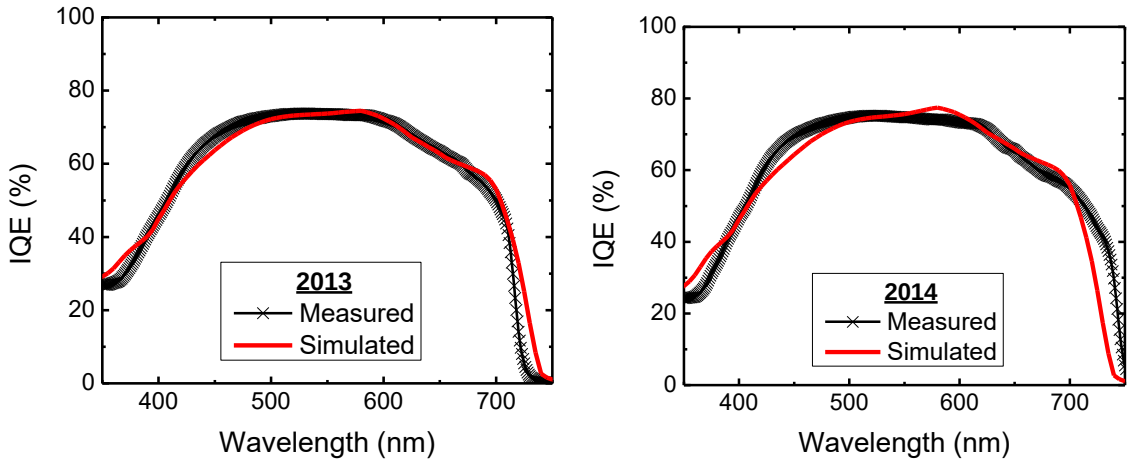

Figure S3. Simulation (red) compared to measured (black crosses) IQE for previously published 1J GaAsP cells from 2013[3] (left) and 2014[4] (right). Differences between simulations and measurements are due to inaccuracies in optical constants for InGaP window layer compositions used in these solar cells.

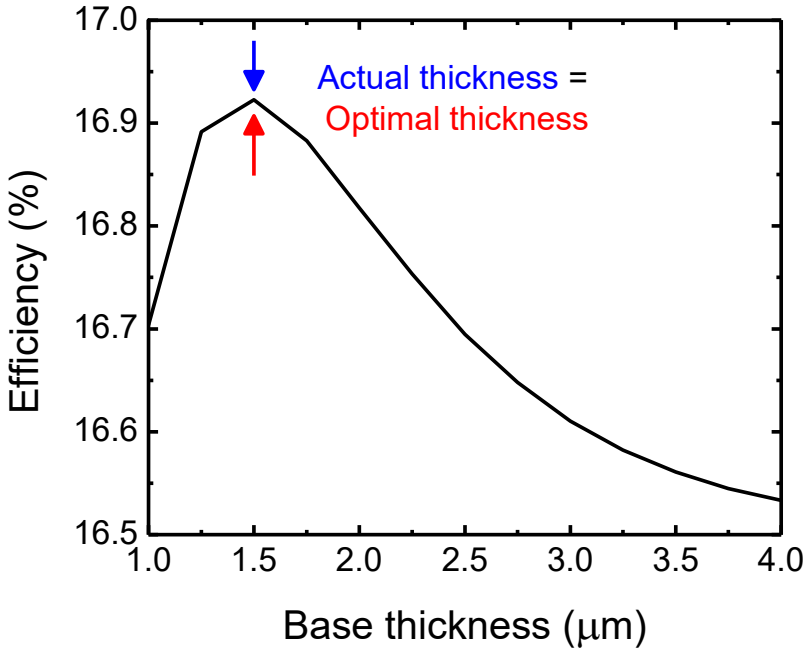

Figure S4. Simulation of our 1J GaAsP solar cell efficiency as a function of GaAsP base thickness, given a τ_n of 0.4 ns, and additionally assuming a grid coverage of 1%.

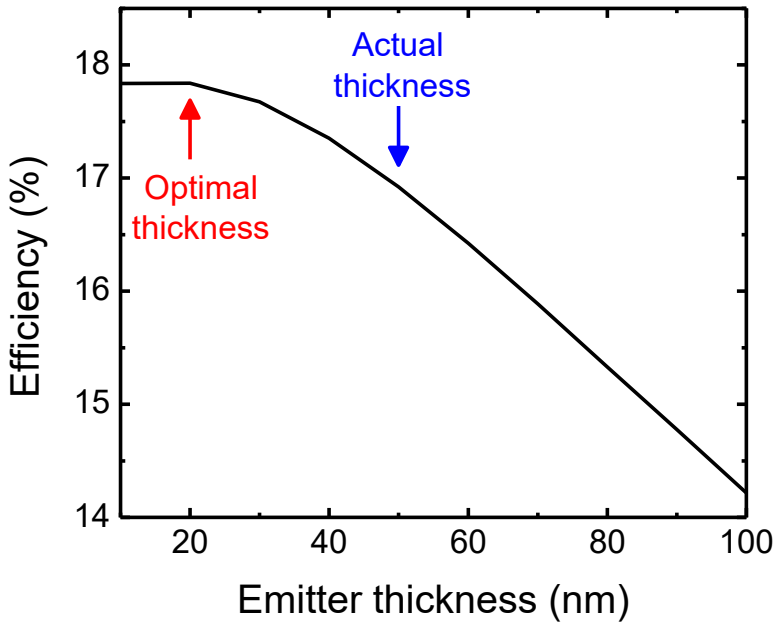

Figure S5. Simulation of our 1J GaAsP solar cell efficiency as a function of GaAsP emitter thickness, given a τ_p of 15 ps, and additionally assuming a grid coverage of 1%.

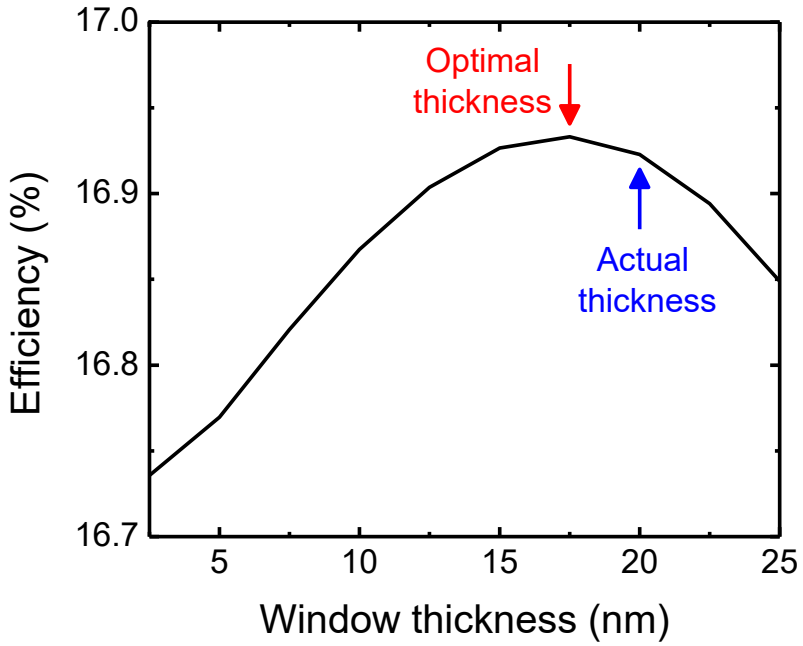

Figure S6. Simulation of our 1J GaAsP solar cell efficiency as a function of InAlP window layer thickness, given a window layer τ_p of 0.01 ps, and additionally assuming a grid coverage of 1%.

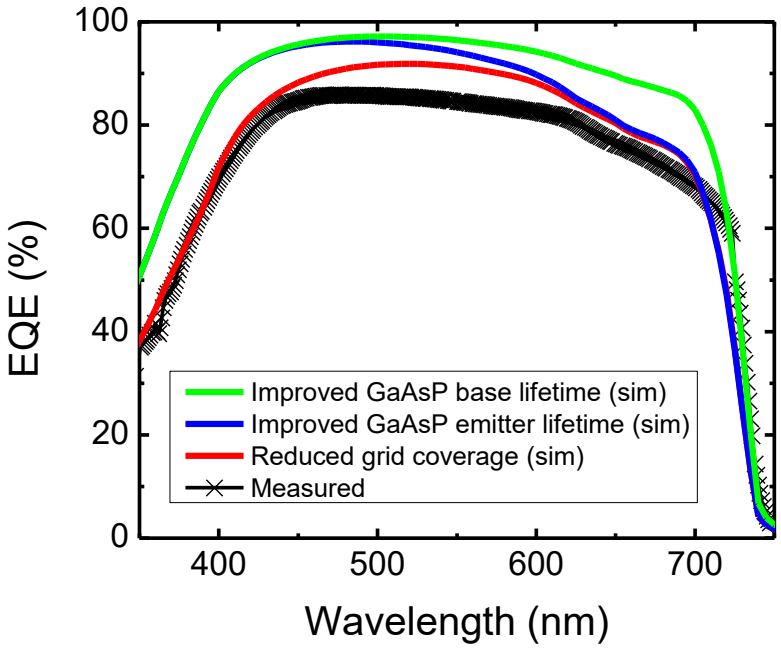

Figure S7. Simulation of our 1J GaAsP solar cell EQE with each successive improvement discussed in Figure 4 in main text: measured (black crosses), reduced grid coverage from 8% to 1% (red), improved GaAsP emitter thickness from 50 nm to 30 nm and τ_p from 15 ps to 60 ps (blue), and improved GaAsP base thickness from 1.5 µm to 2.3 µm and τ_n from 0.4 ns to 1.6 ns (green).

Future ARC Considerations for GaAsP/Si Tandems. A re-designed ARC will be necessary to realize a high-efficiency tandem in a commercial manufacturing environment. Our ARC is optimized for energies greater than $E_{g,\ GaAsP}$ using ZnS and MgF_2. MgF_2 is not often used commercially due to the potential variability in its optical constants[5]; our ARC, however, showed no noticeable change in performance in the two months stored in ambient conditions between

deposition and device certification. To circumvent this potential challenge, a similarly high-performing ARC could be developed for a monolithic GaAsP/Si tandem optimized for energies greater than $E_{g, Si}$ = 1.12 eV with more commercially utilized materials, such as TiO_2 and Al_2O_3 (Figure S8). Our preliminary optimization of a 4-layer TiO_2/Al_2O_3 ARC predicts an AM1.5G-weighted average reflectance of 2.3% in the relevant wavelength range of 350-1110 nm; while the AM1.5G-weighted average reflectance of this 4-layer ARC is slightly less than that of our deposited 2-layer ARC, the latter was optimized for our cell's specific EQE, while this preliminary 4-layer TiO_2/Al_2O_3 ARC was coarsely refined to minimize average reflectance as a proof of concept.

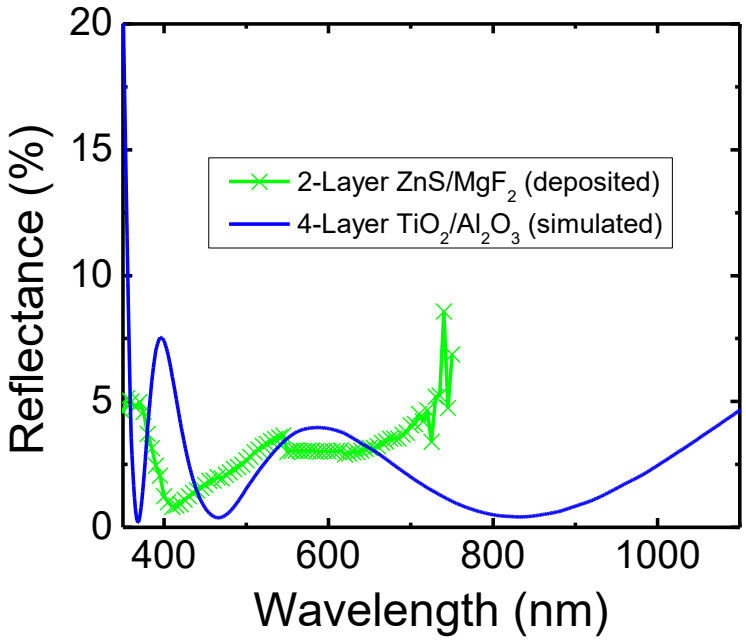

Figure S8. Measured reflectance of the 2-layer ZnS/MgF_2 ARC optimized for our record 1J GaAsP device (green crosses) compared to the simulated 4-layer TiO_2/Al_2O_3 ARC (blue) preliminarily optimized to minimize average reflectance for energies greater than $E_{g, Si}$ for a GaAsP/Si tandem.

Experimental Methods

Growth. Our solar cell materials were grown in a Veeco Mod GEN II solid source molecular beam epitaxy system which was equipped with Al [United Mineral & Chemical Corp (UMC), 99.99995% (6N5) pure, ALR610I1335], Ga (UMC, 7N pure, GA725), In (UMC, 7N pure, IN710A), As (UMC, 7N5 pure, A8EP385), and P (UMC, 7N pure, YC2014-0022) sources and Si (Atomergic Chemetals Corp., 6N pure, SI-0456) and Be (Materion, 4N pure, 356990 000010) dopants, as described elsewhere.[3, 6] Valved As and P sources were thermally cracked into dimer beam fluxes. Auxiliary ionization gauges were used for real-time monitoring of the anion flux ratio during growth. Our devices were co-grown on cleaved pieces of bulk GaP (ITME, Warsaw, Poland) and GaP/Si templates ($NAsP_{III-V}$ GmbH, Marburg, Germany). These templates, described elsewhere[6, 7], consist of a built-in epitaxial silicon p-n junction, followed by a pseudomorphically strained 40 nm n-GaP layer (Figures 1a and 2a) grown on a 300 mm Czochralski p-Si substrate. The exact (001) Si substrate was 775 μm thick and lightly boron-doped (~2×10^{15} cm^{-3}, 8-12 Ω-cm). The epitaxial 200 nm phosphorus-doped n-Si emitter and 40 nm n-GaP window layer of the GaP/Si templates had doping levels of 3×10^{18} cm^{-3} and 3×10^{19} cm^{-3}, respectively (Figure 2a). These GaP/Si templates were cleaved into smaller pieces prior to III-V MBE growth. Before loading into the MBE, the GaP/Si templates were pre-cleaned for 5-7 seconds in 1:2:2 HNO_3:HCl:H_2O. Prior to growth, substrates underwent a 7 hr 200°C bake to remove water from the surface, followed by a shorter ~2 hr 300°C bake to remove hydrocarbons and any remaining water. Lastly, substrates were baked for 20 min at 640°C under a P_2 overpressure to remove surface oxides prior to epitaxial growth.

The pseudomorphically strained GaP was relaxed through the growth of a 500 nm GaP buffer layer using optimized growth conditions.[6] To grade to the required composition, a

$GaAs_yP_{1-y}$ graded buffer (Figures 1a and 2a) was grown with 130 nm-thick steps at 1 μm/hr, 0.80 % misfit/μm, 600°C, and with V/III ratios ranging from 10 to 30. The $GaAs_{0.76}P_{0.24}$ solar cell was grown at 1 μm/hr, V/III≈20, and 575°C. $In_{0.34}Al_{0.66}P$ window and $In_{0.36}Ga_{0.64}P$ back surface field (BSF) layers were used to clad the active region of device for surface & interface passivation; these layers were grown at 0.4 μm/hr and 460°C with a V/III ratio of 18. The MBE-grown n-GaP buffer and n-GaAsP graded buffer on the Si device (Figure 2a) both utilized a 5×10^{18} cm^{-3} doping level.

Fabrication. Solar cells were fabricated in a cleanroom using common photolithography, wet-etching, and e-beam evaporation techniques. Acetone (KMG, 99.5% pure, 200400) and isopropyl alcohol (KMG, 99.5% pure, 200440) were used to clean the semiconductors. Photolithography was performed with positive Shipley S1813 and image reversal AZ 5214 resists and Shipley Microposit MF319 developer using a Laurel WS-400 6NPP spinner and EVG 620 Contact/Proximity Mask Aligner. Device mesa area of the GaAsP top cell was defined by wet chemical etching past the InGaP back surface field layer using a 2:1:50 ammonium hydroxide (J. T. Baker, 28.6% NH_4OH, JT-9721-06):hydrogen peroxide (J. T. Baker, 30-32% H_2O_2, JT-2204-01):deionized water solution for arsenide and mixed anion layers. Concentrated hydrochloric acid (Macron Fine Chemicals, 36.5-28.0% HCl, 2515-46) was used to etch phosphide layers. Device area of the 1J Si bottom cell was defined by an optical aperture and was diced for isolation from the as-fabricated sample.

Metallization was performed via lift-off of e-beam evaporated metal stacks. On the GaAsP device, a Denton Infinity 22 E-Beam Thermal Evaporation System was used to deposit nominal metal stack thicknesses of 100 nm AuGe (88/12 wt%, Kurt J. Leskar, 4N pure, EVMAUGE40EXE) / 20 nm Ni (Kurt J. Leskar, 4N5 pure, EVMNI45EXEB) / 100 nm Au (Kurt

J. Lesker, 5N pure, EVMAUXX50G) for contacts to n-type layers and 10 nm Cr (Kurt J. Lesker, 3N5 pure, EVMCR35D) / 200 nm Au for p-type layers. Two top contacts were placed at the planes of the n-GaAs and p-GaAsP layers that sandwich the solar cell clads; these two layers are highly doped ($n_0 = p_0 = 1\times10^{19}$ cm^{-3}) to facilitate contact formation. On the Si bottom cell, 200 nm of Al was deposited on the backside of the wafer (Temescal Six Pocket E-Beam Evaporation System) and was annealed at 700°C for 10 min under an N_2 flow rate of 500 sccm to form a BSF; no back surface passivation was employed prior to MBE growth.[8] The Si cell was not textured (Figure 2a). The bottom metal stack with nominal thicknesses of 20 nm Ni / 50 nm Au was deposited on the Al BSF using a CHA SEC-600 E-Beam Evaporator; an identical top metal contact as was used on the GaAsP top cell was deposited onto the top-most n-GaAsP contact layer of the Si bottom cell (Figure 2a). The GaAsP ARC was thermally evaporated (NRC Varian 3115 Vacuum Deposition System) with measured thicknesses of 29.4 nm ZnS (Materion, 4N pure, Z-2028) / 81.4 nm MgF_2 (Materion, 5N pure, M-2010); metal contacts on the GaAsP cell were protected from ARC deposition for device contacting via photolithography and lift-off. The bottom cell ARC of 110 nm SiN_x was deposited via plasma-enhanced chemical vapor deposition (STS Mesc Multiplex PECVD).

Characterization. The GaAsP solar cell prior to ARC deposition and the Si solar cell both before and after ARC deposition were measured as follows. LIV was taken under approximate AM1.5G illumination conditions (ABET Technologies 10500 solar simulator) and EQE measurements were performed in a PV Measurements QEX7 system; the specular reflectance measurements of the Si solar cell were taken on the QEX7 as well. The bandgap was determined from the cut-off wavelength of the EQE.[9] TDD was determined via electron beam-induced current (EBIC) mapping in a FEI XL 30 scanning electron microscope with accelerating

voltages of 10.5-12.5 kV. X-ray reciprocal space mapping (Rigaku SmartLab) confirmed material compositions and that our cells exhibited strain relaxation greater than 95% at 300 K.

Specular reflectance measurements of the GaAsP device were taken before and after ARC deposition on a custom-built tool under chopped, monochromatic light for the determination of IQE and an optimal ARC design. Optical constants for InAlP and GaAsP of nominally similar compositions to those used in our solar cell designs were determined by spectroscopic ellipsometry (J.A. Woollam, ESM-300). ARC modelling was conducted using TFCalc. Numerical 2D simulations of device results were computed using Silvaco TCAD Atlas.

The LIV and EQE of our record-efficiency AR-coated GaAsP on GaP/Si solar cell were third-party certified by the PV Performance Characterization Team at the National Renewable Energy Laboratory. LIV was measured using an ABET solar simulator with an intensity set using a spectroradiometer, primary reference cells, and spectral mismatch correction factors for the AM1.5G spectrum. EQE was measured on a grating monochromator system. Device area of our Si cell was nominally 0.1225 cm^2 and that of our certified GaAsP top cell was measured as the mesa area, as viewed under a Nikon NEXIV VMR-3020-LU microscope, which was found to be 0.03915 cm^2 ± 0.3%.

References

(1) Conrad, B.; Lochtefeld, A.; Gerger, A.; Barnett, A.; Perez-Wurfl, I. Optical Characterisation of III-V Alloys Grown on Si by Spectroscopic Ellipsometry. *Sol. Energy Mat. Sol. Cells* 2017, *162*, 7-12.

(2) Yu, Z.; Leilaeioun, M.; Holman, Z. Selecting Tandem Partners for Silicon Solar Cells. *Nat. Energy* 2016, *1*, 16137.

(3) Lang, J. R.; Faucher, J.; Tomasulo, S.; Nay Yaung, K.; Lee, M. L. Comparison of GaAsP Solar Cells on GaP and GaP/Si. *Appl. Phys. Lett.* 2013, *103*, 092102.

(4) Nay Yaung, K.; Lang, J. R.; Lee, M. L. *Towards High Efficiency GaAsP Solar Cells on (001) GaP/Si*, Proc. 40th IEEE Photovolt. Spec. Conf., Denver, CO, USA, 2014; pp 0831-0835.

(5) Ogura, S.; Sugawara, N.; Hiraga, R. Refractive Index and Packing Density for MgF_2 Films: Correlation of Temperature Dependence with Water Sorption. *Thin Solid Films* 1975, *30*, 3-10.

(6) Nay Yaung, K.; Vaisman, M.; Lang, J.; Lee, M. L. GaAsP Solar Cells on GaP/Si with Low Threading Dislocation Density. *Appl. Phys. Lett.* 2016, *109*, 032107.

(7) Volz, K.; Beyer, A.; Witte, W.; Ohlmann, J.; Németh, I.; Kunert, B.; Stolz, W. GaP-Nucleation on Exact Si (001) Substrates for III/V Device Integration. *J. Cryst. Growth* 2011, *315*, 37-47.

(8) Del Alamo, J.; Eguren, J.; Luque, A. Operating Limits of Al-alloyed High-Low Junctions for BSF Solar Cells. *Solid State Electron.* 1981, *24*, 415-420.

(9) Todorov, T. K.; Gunawan, O.; Gokmen, T.; Mitzi, D. B. Solution-Processed $Cu(In,Ga)(S,Se)_2$ Absorber Yielding a 15.2% Efficient Solar Cell. *Prog. Photovolt. Res. Appl.* 2013, *21*, 82-87.

National Renewable Energy Laboratory Characterization Certificate of GaAsP Top Cell

Yale

GaAsP Cell

Device ID: 3B 160527
Jul 12, 2016 15:28
Spectrum: ASTM G173 global

Device Temperature: 24.8 ± 0.5 °C
Device Area: 0.03915 cm^2 ± 0.3 %
Irradiance: 1000.0 W/m^2

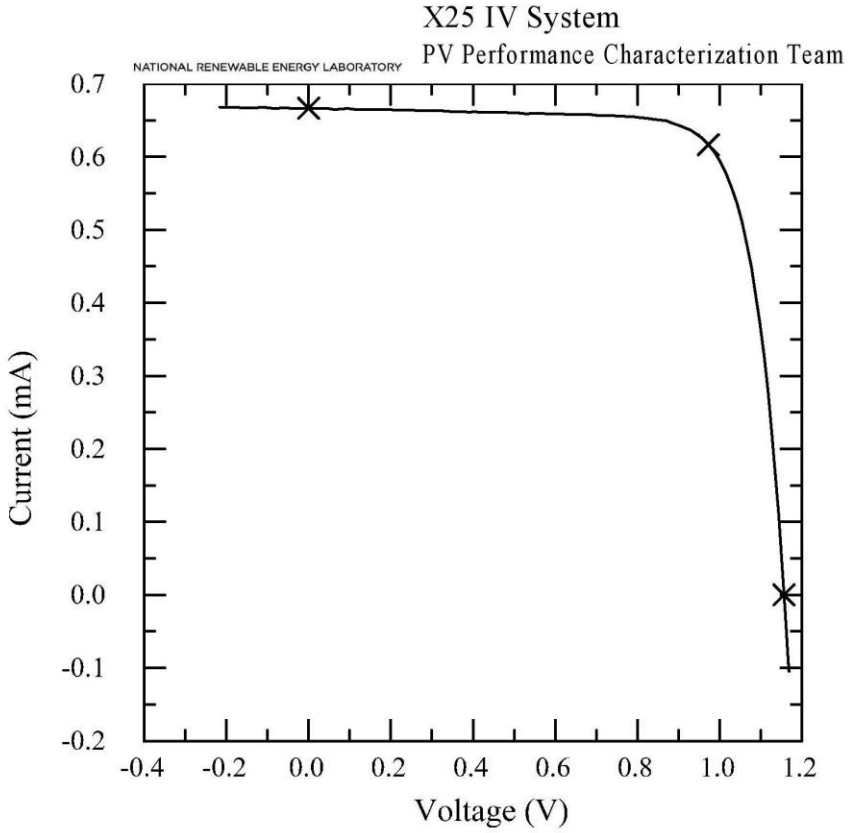

V_{oc} = 1.1569 V ± 0.2%
I_{sc} = 0.66622 mA ± 2.2%
J_{sc} = 17.018 mA/cm^2 ± 2.2%
Fill Factor = 77.85 % ± 0.4%

I_{max} = 0.61643 mA ± 2.2%
V_{max} = 0.9734 V ± 0.2%
P_{max} = 0.60003 mW ± 2.2%
Efficiency = 15.33 % ± 2.2%

Continuous illumination.
Reference cell located 5cm from test device. Add 1% to current uncertainty.